SIMULATION OF EXPERIMENTAL VISUALIZATION METHODS FOR COMPUTATIONAL FLUID DYNAMICS RESEARCH

Y. TAMURA and K. FUJII

The Institute of Space and Astronautical Science, Yoshinodai 3-1-1, Sagamihara, Kanagawa, 229 Japan

(Received 3 February 1993; Revised 10 October 1993; in final form)

SUMMARY

In the present paper, visualization techniques in fluid dynamic experiments such as Schlieren photograph are numerically simulated so that the same output as the experimental flow visualization can be obtained from the computed results for the fair comparison. Numerical methods to simulate optical visualizations, that are Schlieren photograph, shadowgraph and interferogram, are considered. Some examples of pictures obtained by the present methods show the importance of the simulations of visualization techniques for the correct comparisons of the computations and experiments.

1. INTRODUCTION

As the scale of fluid simulations becomes larger with the aid of supercomputers, importance of the postprocess of such simulations begins to be recognized.

The postprocess in computational fluid dynamics (CFD) has two purposes. One is to examine computed results to confirm that they give physically reliable answers. The other is to analyse the computed flow fields and extract flow physics under the assumption that the computations are reliable.

In order to confirm the reliabilities of the computed results, comparison with the experiment is useful. Historically from the very early stage of the CFD, comparisons by numbers such as forces, moments and pressure distributions have been frequently made. Comparisons by numbers have no ambiguities and they might be sufficient when the simulated flow fields are relatively simple such as the flows over an airfoil.

For complicated flow fields involving shock waves, separations, vortices and their interactions, entire flow fields should be compared. Comparison with the visualized image in the experiment is useful for this purpose. Computed results must then be visualized for the comparison with visualized images taken in experiments. Visualization of computed results is an important part of the postprocesses and is becoming popular with the progress of computer graphics (CG) and graphics workstations. However, much more attention should be paid to the visualization of computed results. For instance, the density contour plots at a certain plane (plane

of symmetry in the case of axisymmetric body, for instance) in computations are often compared with the Schlieren photographs taken in the experiments. Schlieren photographs are not the visualized image of the density within the plane although it is true that the density distribution is a key parameter for the Schlieren photographs. There is difference between the Schlieren photograph and the density contour plots and this differences might introduce misunderstanding of the computed result in the comparison with the experiments.

Plotting density contours within a plane is an easy task on the computer and they are sometimes satisfactory as a postprocess. However, one advantage of the CFD is availability of the information for entire flow fields. It is possible to numerically simulate the process of experimental visualizations and obtain the same sort of pictures from the computed results as those from the experiments. These pictures can be compared with the experiments directly.

In the present paper, numerical methods to simulate visualization process in experiments (Tamura *et al.* (1990a)) are discussed. The visualization methods in this context are limited to the optical methods, namely Schlieren photograph, shadowgraph and interferogram. In the next section, the principles of optical methods are briefly reviewed. The numerical methods to simulate each experiments are described with some examples in the third section. Nonlinear effects of the deflection of light are also investigated and the last section concludes the present work.

2. PRINCIPLES OF OPTICAL VISUALIZATION METHODS

2.1. Deflection of Ray of Light

The basis of optical visualization experiments is that the velocity of light differs according to the density of medium through which the light goes and as a result, the deflection rate of light changes (Liepmann *et al.* (1956)). It can be written as,

$$n = \frac{c_0}{c} \cong 1 + \beta \frac{\rho}{\rho_s} \tag{1}$$

where n is deflection rate, c is speed of light, $(\cdot)_0$ indicates a state of vacuum and $(\cdot)_s$ indicates a standard state. Although this equation is a first-order approximation, the higher-order error is negligibly small in the case of air. β is a non-dimensional parameter and $\beta = 0.000291 \sim 0.000297$ according to the wavelength.

When variation of density exists in the flow field, a wavefront of light turns due to the difference of local speed of light. Figure 1(a) shows the schematic picture of the turning of the wavefront of light, where w denotes the wavefront and r denotes the direction of light. Let the turning angle of wave front ϕ, a coordinate along the ray of light ξ and normal to the ray η, as shown in Figure 1(b), the deviation of the

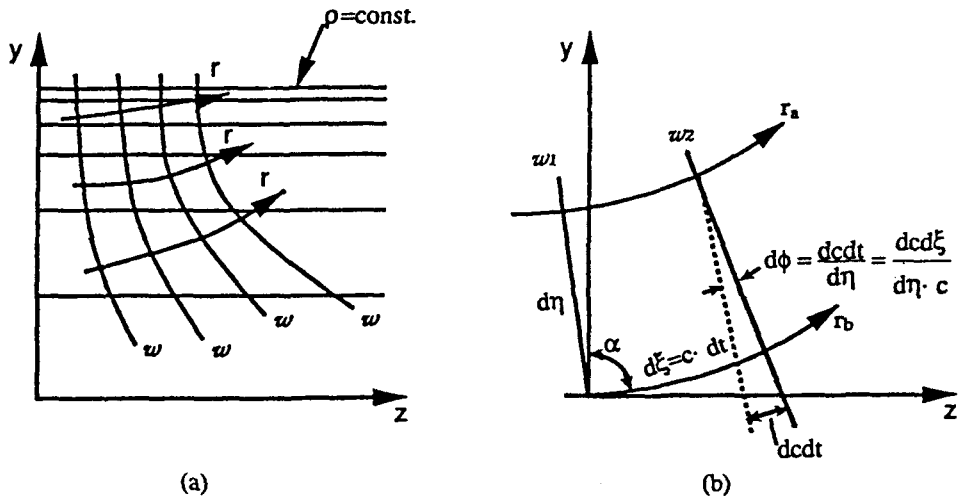

Figure 1 Deflection in density field (Liepmann *et al.* (1956)) (a) Rays (r) and wavefronts (w) (b) Orthogonal networks of rays and wavefronts.

turning angle ϕ due to the difference of the local speed of light can be written as,

$$\Delta\phi = \frac{\Delta c \cdot \delta t}{\Delta \eta} = \frac{\Delta x \cdot \Delta \xi}{c \cdot \Delta \eta}$$

and,

$$\frac{d\phi}{d\xi} = \frac{1}{c}\left|\frac{dc}{d\eta}\right| = \frac{1}{n}\left|\frac{dn}{d\eta}\right| \tag{2}$$

With ρ, the density normalized by the standard state, the deviation of ϕ in y direction in Figure 1(b) can be written as,

$$d\phi = \frac{\beta}{n}\frac{\partial \rho}{\partial \eta}\, d\xi \approx \frac{\beta}{n}\frac{\partial \rho}{\partial y}\, dz \tag{3}$$

Assume that the ray of light comes along z axis and the light deflects only in y direction, ε, the deflection angle of light to z axis can be written as,

$$\varepsilon = \int_{\text{ray}} d\phi \tag{4}$$

If the deflection is small and the light path can be approximated as $y = y_1$,

$$\varepsilon = \int_0^L \left(\frac{\beta}{n}\frac{\partial \rho}{\partial y}\right)_{y_1} dz \tag{5}$$

where L is the length where the light experience the density gradients (the width of the test section, for instance). Note that this approximation is not necessarily exact for strong density gradients, such as shock waves and boundary layers. When the flow field is two-dimensional and constant in z direction, and $n \approx 1$,

$$\varepsilon = L\beta\left(\frac{\partial \rho}{\partial y}\right)_{y1} \qquad (5)'$$

Consequently, *the deviation of light is proportional to the density gradient in its direction*, and this is the basis of the optical visualization methods.

The following discussion will be based on equations (5) and (5)′ though there are some approximations between equation (4) and equation (5) (or equation (5)′). Effects of the approximations, in other words non-linear effects, will be discussed in the fourth section.

2.2. *Principle of Schlieren Photography*

The principle of Schlieren photograph can be described based on the discussion in the previous section. Figure 2 shows an optical system for Schlieren photograph. The deviation only in the y direction is considered for simplicity.

When setting a light source of a finite width at the focal point of lens L_1, the uniform parallel light goes through the test section, is deflected in lens L_2, and makes the image of the light source at the focal point of the lens L_2. Lens L_3 make the light parallel again and a screen is illuminated. The screen is set at a certain location where the image of the test section is focused.

When the density varies in the test section, the light turns according to the density gradient. Since the screen is placed in the focal point, the light, which goes through the test section and the lens L_2, illuminates the same position of the screen as in the case of no density variations. Thus the lightness on the screen is constant in the Schlieren system even though there are some density gradients in the test section.

On the other hand, when a plate (usually a knife edge) is placed as to hide half of the light at the point where the light source focuses, the intensity of the light is reduced to be its half and then a lightness on the screen also becomes half in the case of the constant density. When there are density gradients in the test section,

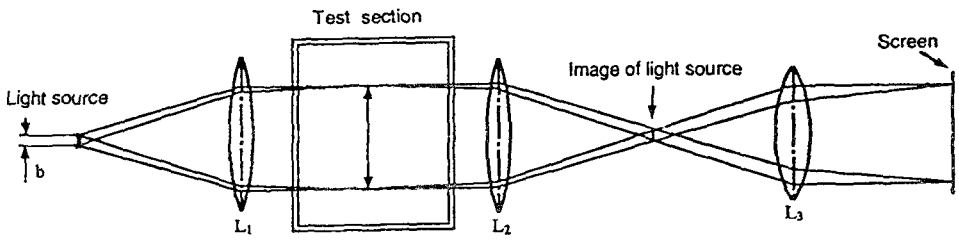

Figure 2 Schematic picture of Schlieren system (Liepmann *et al.* (1956)).

the image of the light source is shifted at the knife edge and the blocked area of the light is not necessarily half and is dependent on the rate of deflection of the light. Hence, let f_2 the length of the focus of the lens L_2, b the width of the light source and I_0 the intensity without the knife edge, and using the rate of deflection ε, the intensity on the screen becomes,

$$I = I_0\left(0.5 + \frac{f_2}{b}\,\varepsilon\right) \tag{6}$$

in two-dimensional flow,

$$I = I_0\left(0.5 + \frac{f_2}{b}\,L\beta\left(\frac{\partial\rho}{\partial y}\right)_{y_1}\right) \tag{6}'$$

Note that $0 \leqslant I \leqslant I_0$. The intensity outside of this range occurs when the light deflects too much and is completely hidden by the knife edge or completely clear from the knife edge. Within this range, the intensity of the screen is proportional to the density gradient. Though the light may turn to x direction with the density variations in x direction, $\partial\rho/\partial x$ has no effects to the intensity since only y direction is effective for the knife edge placed horizontally. If the knife edge is set vertically, only the density gradient in x direction is observed.

Colour filters are often used instead of knife edges. The colour filters are usually made of three strips of filters, namely, red, green and blue, which are aligned to each other. For example, if the colour of the middle filter be green, and the width of the image of the light source at that point be the same as that of the green filter, then the colour on the screen becomes green mixed with red or blue according to the drift of the light. The rate of mixture is proportional to the density gradient and the resultant colour is linearly proportional to the colour function of so-called Hue. The difference between the knife edge Schlieren and the colour Schlieren is that the intensity of the screen is constant in the case of colour Schlierens and not in the case of knife edge.

2.3. Principle of Shadowgraph

Shadowgraph technique is similar to the Schlieren photograph. The major differences are that no knife edges are used and that the screen is placed out of the focal point. Since the screen is not at the focal point, the light does not come to the same position on the screen when the light is deflected due to the density gradient. Thus the lightness on the screen is not uniform when the deflection of light is not constant as shown in Figure 3, even though the light is not shielded by knife edges. Define the lightness on the screen as I, and since I is proportional to the deviation of the deflection of the light, I can be written as,

$$I \propto \frac{\partial\varepsilon_x}{\partial x} + \frac{\partial\varepsilon_y}{\partial y} \tag{7}$$

where ε_x, ε_y are the deflections of the light in x and y directions, respectively.

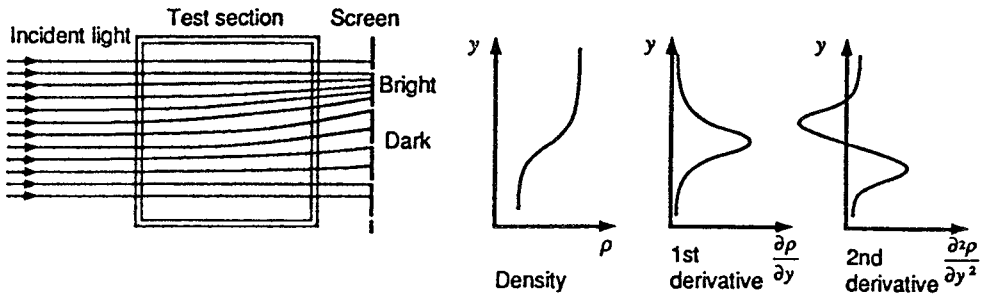

Figure 3 Principle of shadowgraph (Liepmann *et al.* (1956)).

In two-dimensional flows,

$$I \propto \frac{\partial^2 \rho}{\partial x^2} + \frac{\partial^2 \rho}{\partial y^2} \tag{7}'$$

In the case of a shadowgraph, the positions of an image on the screen do not exactly correspond to those in the test section and the image is obviously distorted where the density gradient is strong. Hence the comparison of the shadowgraph images between computations and experiments may be qualitative rather than quantitative.

2.4. Principle of Iterferogram

The principle of interferogram, which is different from either that of Schlieren photograph or shadowgraph, is interference of light. Figure 4 shows the paths of two lights which start from the same source and one of which goes through the test section and the other goes through the reference area. The two lights meet on the screen and the path lengths are the same. When the densities in the test section and in the reference area are different, the effective path lengths differs since the speed of light differs by the principle of equation (1). This can be written as,

$$\Delta L = c_0 \times \left(\frac{L}{c} - \frac{L}{c_0} \right) = nL - n_s L = \beta \frac{\rho - \rho_s}{\rho_s} L \tag{8}$$

where L is the physical path length and $(\cdot)_s$ denotes the standard state in the reference area. Equation (8) shows that the difference of the two path lengths is proportional to the differences of the densities in the test section and in the reference area. The differences of the path lengths causes the black and white stripes on the screen. The drift of the stripe ΔN by the difference of the path lengths can be written with the wavelength of light in standard state λ_s as,

$$\Delta N = \frac{\Delta L}{\lambda_s} = \frac{\beta L}{\lambda_s} \frac{\rho - \rho_s}{\rho_s} \tag{9}$$

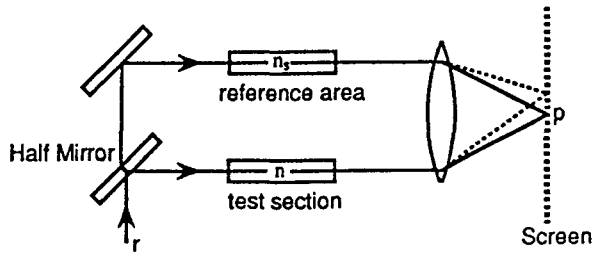

Figure 4 Schematic picture of interferogram (Liepmann *et al.* (1956)).

When ΔN is just an integer, the phases of two lights meet and the screen becomes bright. On the other hand, when the fraction of ΔN is 0.5, the phases are reverse and the screen becomes dark.

The interferogram is set either to have some stripes even in uniform flow and distort them by the variation of density or to have no stripes (or one) in uniform flow. The former setting is called finite fringe and latter called infinitesimal fringe. In the case of the infinitesimal fringe, ΔN is just as written in equation (9) and ΔN becomes $N_s(x,y) + \Delta N$ in finite fringe, where $N_s(x,y)$ is the stripes in uniform flow.

3. SIMULATION OF EXPERIMENTAL VISUALIZATIONS BY COMPUTERS

3.1. Simulation of Schlieren Photograph

Two-dimensional flow fields are considered first. The lightness on the screen I follows equation (6)′ as,

$$I = I_0\left(F_n + \frac{f_2}{b} L\beta \frac{\partial \rho}{\partial y}\right)$$

Here the lightness on the screen with no density gradient is denoted by F_n which is supposed to be 0.5 in the previous section. Suppose the lightness ranges from 0 to 1 and denote F_0 the factor for the density gradient, then the equation above yields,

$$I = F_n + F_0 \frac{\partial \rho}{\partial y} \tag{10}$$

Thus the lightness of a certain point on the screen is obtained by the density gradient normal to the knife edge from the computed result. There are two parameters in equation (10). F_n can be 0.5 usually. When the density gradient is biased to positive or negative value, F_n can be changed to use the lightness range

effectively. On the other hand, F_0 corresponds to the sensitivity of the Schlieren system and is thus variable. It is usually set empirically with the magnitude of density gradient, though it could be calculated directly from the parameters of the experiment system, such as the features of the lens.

In the case of colour Schlierens, hue corresponds to the lightness as,

$$H = F_n + F_0 \frac{\partial \rho}{\partial y} \tag{11}$$

Hue is a periodic function and generally red corresponds to 0 (and 1), green to 1/3 and blue to 2/3. Hence F_n should be 1/3 and F_0 should be set such that $0 \leqslant H \leqslant 2/3$ when the sequence of the colour of the filter is red, green and blue.

The way to draw pictures by computer graphics (CG) after obtaining the lightness or colours is not the focus of the present paper. Briefly speaking, recent CG softwares can fill out the inside of the three-dimensional polygons with smooth colour gradations from the coordinates and the RGB values at the vertices of the polygons. The RGB value at the vertices are obtained from equation (10) or (11) using finite difference approximations and thus the programming is not a difficult task. Note that lightness is linearly interpolated by CG but the hue is not since the colour gradations are achieved by linear interpolations of RGB values and hue is not a linear function of RGB. As a result, the order of accuracy of the colours inside grids (polygons) can be less than first-order though it might be accurate enough for the comparisons of images.

The flow field about a two-dimensional supersonic air intake is taken as an example. Figure 5(a) shows a colour Schlieren picture in the experiment (Sakata *et al.* (1989)) and Figure 5(b) shows a simulated colour Schlieren picture from the computed result with the same condition (Kuroda *et al.* (1991)) as the experiment. Density contour surface plots are shown in Figure 5(c) as a reference. The simulated Schlieren pictures are obviously better for the comparison with experiments than the density contours.

In the case of three-dimensional flows, under the assumption that $n \sim 1$, Equations (4) and (6) give,

$$I = I_0\left(F_n + \frac{f_2 \beta}{b} \int_0^L \frac{\partial \rho}{\partial y}\, \mathrm{d}z\right)$$

and re-written as,

$$I = F_n + F_0 \int_0^L \frac{\partial \rho}{\partial y}\, \mathrm{d}z \tag{12}$$

This integral has to be numerically evaluated in the case of three-dimensions.

Practically, the integration is done by the following manner. First, the structured grid that we usually used is divided into five tetrahedra to simplify the problem (Figure 6). Then tetrahedra that the traced ray of light goes through are searched.

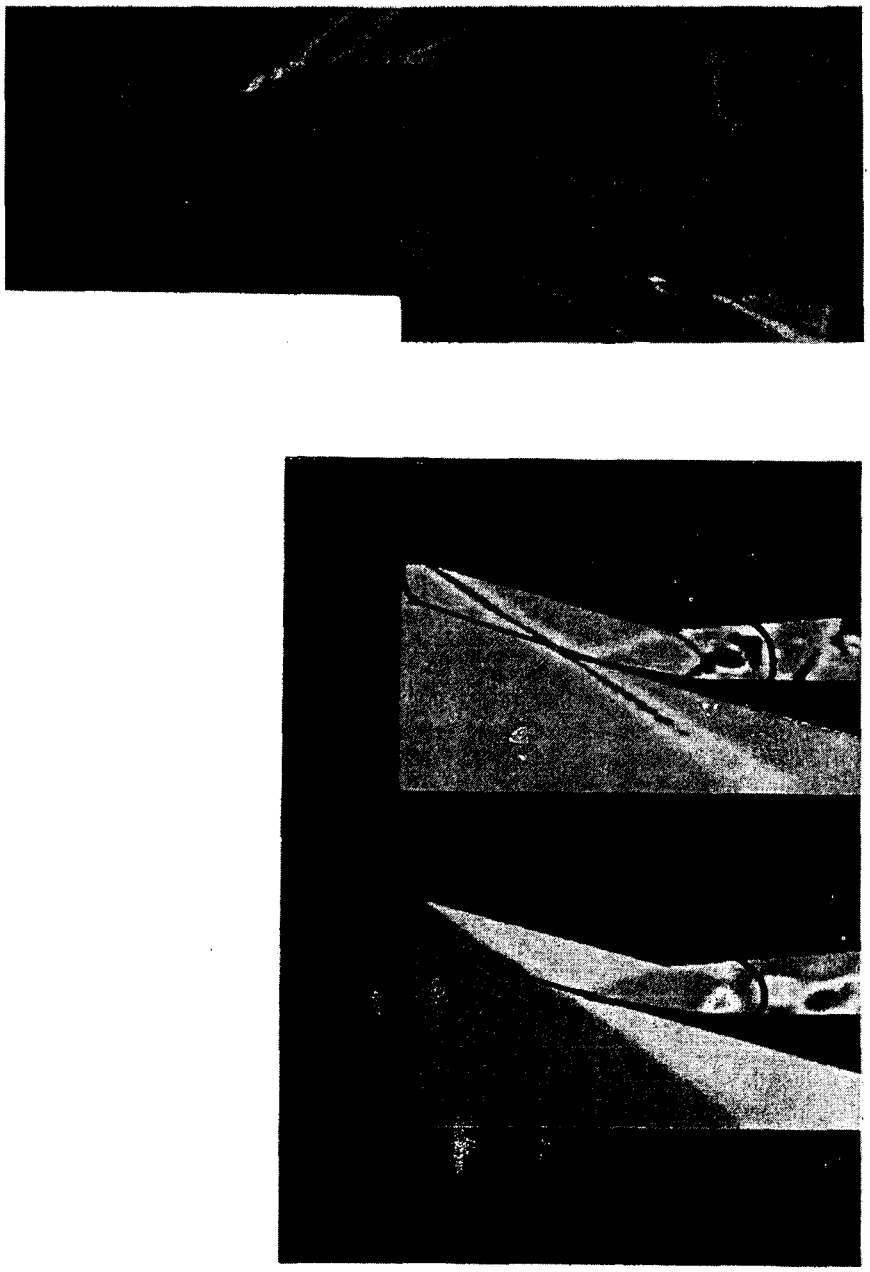

Figure 5 Flow around a two-dimensional supersonic air inlet (a) Experimental colour schlieren photograph (Sakata *et al.* (1989)) (b) Simulated color schlieren photograph with computed result (Kuroda *et al.* (1991)) (c) Density contours of computed result (Kuroda *et al.* (1991)). (See color plate I at the back of this issue.)

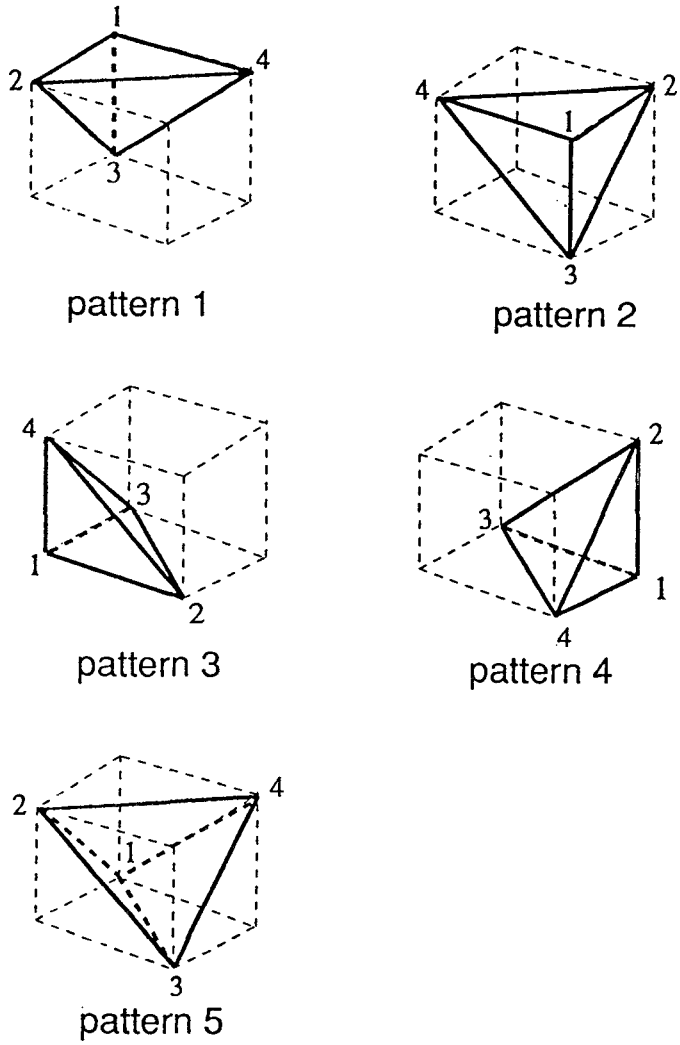

Figure 6 Division of a hexahedron.

The ray comes into the tetrahedron through one face and goes out through one of the other three faces (Figure 7). Since the interpolation inside a tetrahedron can be linear (this is one reason why we do not use hexahedra but tetrahedra), the integration of the density gradient inside one tetrahedron can be written as equation (13).

$$\Delta\rho_t = \frac{1}{2}\left[\left(\frac{\partial\rho}{\partial y}\right)_{\text{in}} + \left(\frac{\partial\rho}{\partial y}\right)_{\text{out}}\right] \times l_t \tag{13}$$

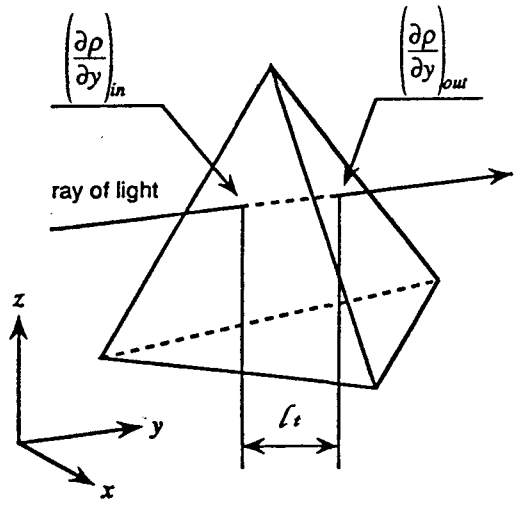

Figure 7 Numerical integration within a tetrahedron.

where $(\cdot)_{in}$ denotes the point where the ray comes in and $(\cdot)_{out}$ the point where the light goes out. l_t is a distance between these two points. This integration is carried out in every tetrahedron that the ray goes through and the integrated density gradients for the tetrahedra are summed up. Finally the integration of that point is approximated as,

$$\int_0^L \frac{\partial \rho}{\partial y} \, d\tilde{z} \approx \sum_t \Delta \rho_t$$

and thus,

$$I = F_n + F_o \sum_t \Delta \rho_t \tag{14}$$

One of practical problems is a search for the tetrahedra. Judgements of intersections between the ray and a randomly selected tetrahedron might require considerable time. However, once one tetrahedron which crosses the ray is found, the tetrahedron into which the ray goes next can easily be found without any searching processes since these tetrahedra share the same face through which the ray goes.

Another problem is a number and positions of ray of lights to be traced. Of course, as the number of rays increases, the resolution of picture increases but the computational time also does. For example, the rays from all of the pixels of the display are ideal, but the number of rays will become up to million and a couple of hours of the CPU time might be required even with current high performance workstations. Therefore the number of rays has to be reduced. Here the rays start only from the grid points of a certain grid surface (practically, the symmetry plane

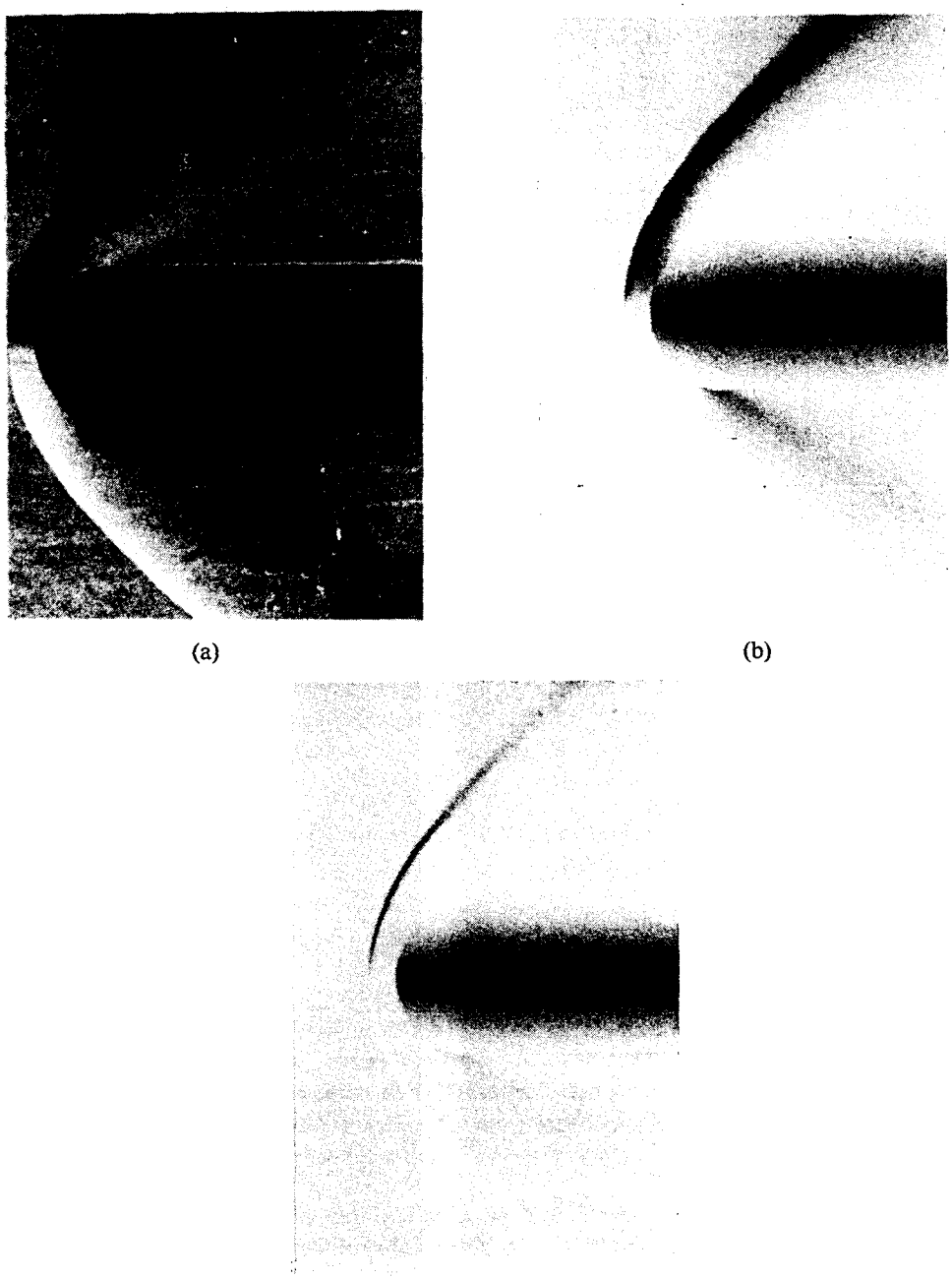

Figure 8 Visualization of flow around a blunt body (a) Experimental Schlieren photograph (Johannesen (1952)) (b) Simulated Schlieren photograph with computed result (Tamura *et al.* (1990b)) (c) Simulated Schlieren photograph with computed result within a plane of symmetry (Tamura *et al.* (1990b)).

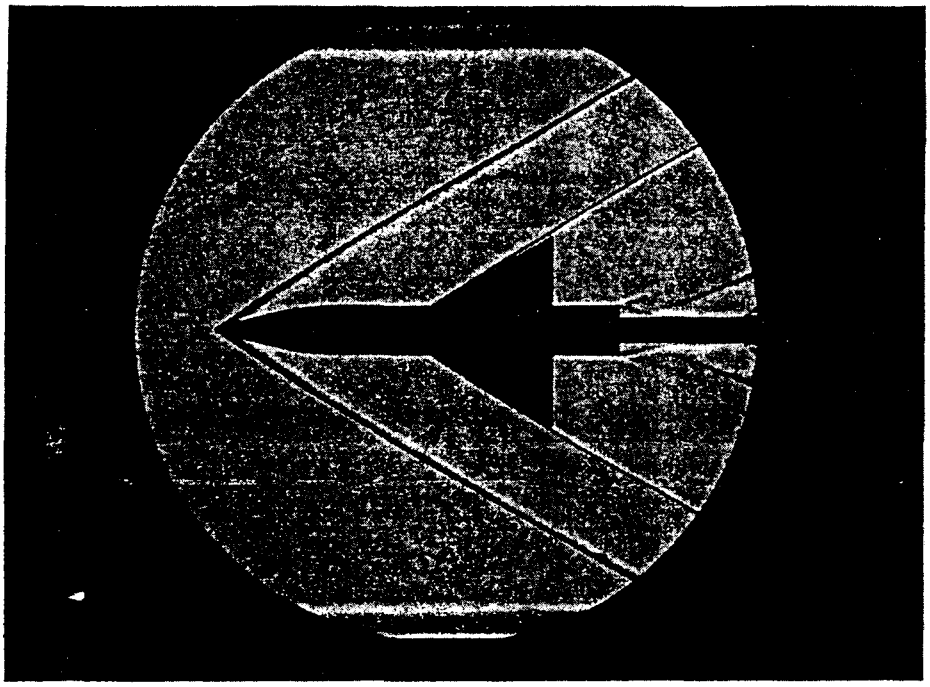

(a)

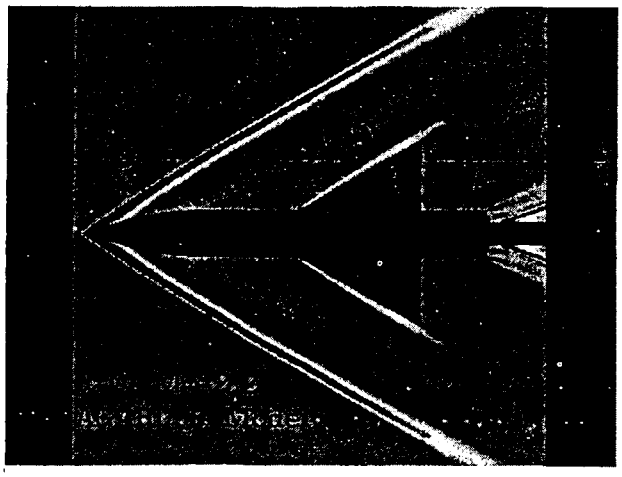

(b)

Figure 9 Visualization of flow around AGARD-B model (a) Experimental colour schlieren photograph (Inatani *et al.* (1990)) (b) Simulated color schlieren photograph with computed result (Tamura *et al.* (1990c)). (See color plate II at the back of this issue.)

is a good choice since its shape corresponds to the Schlieren image). Of course, any other starting points are possible. Once the lightness on the screen is calculated, the CG program paints the surface like the contour surface plots.

Some of the application examples are presented. The first one is a visualization of flow around a hemisphere cylinder ($M_\infty = 1.96, \alpha = 0^\circ$). Figure 8(a) shows a Schlieren photograph in the experiment (Johannesen (1952)) where the density gradient in y direction are visualized. The simulated Schlieren picture from the computed results under the same condition (Tamura *et al.* (1990b)) is shown in Figure 8(b). These two pictures show a good agreement. Two-dimensional Schlieren photograph within a symmetry plane is also simulated with the density gradient in y direction (Figure 8(c)) since properties in symmetry plane are often compared with experiments. Pictures of the experiment and three-dimensionally simulated Schlieren show smooth gradation of lightness behind the shock wave. On the other hand, the lightness suddenly changes after the shock wave in two-dimensional picture. Since the bow shock wave spreads over the cylinder, the ray of light behind the shock wave actually crosses the bow shock wave twice and experiences some density jumps. Experiment and simulated three-dimensional Schlieren photograph include this effect but it cannot be reflected in the picture of the symmetry plane. This three-dimensional effects may become important in the case of more complex flow fields.

As an example of practical configurations, the supersonic flow around a AGARD_B supersonic wind tunnel calibration model is presented. The free stream Mach number is 2.2 and the angle-of-attack is 0 degrees. Figure 9(a) shows the experimental colour Schlieren picture (Inatani *et al.* (1990)) and Figure 9(b) shows the simulated three-dimensional colour Schlieren picture of a computation (Tamura *et al.* (1990c)). Shock waves from the nose and wing leading edge, expansion wave after the body and reflected shock wave on the sting are well resolved.

3.2. Simulation of Shadowgraph

In a shadowgraph, the lightness is proportional to the gradient of the deflection of light without considering distortion of images. In two-dimensional flow, the lightness can be written with the lightness of constant deflection of light I_0 as,

$$I = I_0\left[1 + F_s\left(\frac{\partial^2 \rho}{\partial x^2} + \frac{\partial^2 \rho}{\partial y^2}\right)\right] \tag{15}$$

F_s is a parameter determined by the distance between the screen and the focal point and other factors, and is generally negative, as shown in Figure 3, and the screen becomes dark when the second derivative is positive. Thus the actual numerical procedure is simply calculating the second derivative of the density at each grid point using finite difference approximations. As a difference from the Schlieren photograph, $I > I_0$ is possible when the rays are concentrated. Since the maximum intensity of the display is finite, the parameters should be chosen to control the range of I.

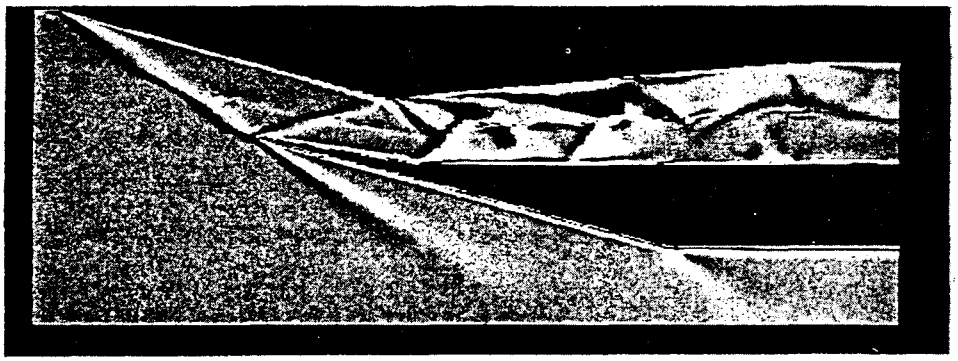

Figure 10 Simulation of shadowgraph for computed result of two-dimensional supersonic air inlet (Kuroda *et al.* (1991)).

Figure 10 shows the simulated shadowgraph picture with the computed result of the flow around the supersonic inlet taken in the previous section as an example.

In three-dimensional flow, Equation (7) can be re-written as,

$$I = I_0\left[1 + F_s\left(\frac{\partial \varepsilon_x}{\partial x} + \frac{\partial \varepsilon_y}{\partial y}\right)\right] \tag{15}'$$

note that,

$$\varepsilon_x = \int_0^L \beta \frac{\partial \rho}{\partial x}\, dz, \qquad \varepsilon_y = \int_0^L \beta \frac{\partial \rho}{\partial y}\, dz$$

Therefore the density gradients in both x and y directions are integrated separately and then ε_x and ε_y are differentiated. Tracing of the rays can be done by the same manner as the Schlieren photograph. Shadowgraphs of an experiment (Lehr (1972)) and a corresponding computation (Matsuo *et al.* (1991)) of the flow field where unstable combustion occurs between a blunt body and a bow shock wave in pre-mixed supersonic flow are shown in Figure 11.

3.3. Simulation of Interferogram

The principle of interferogram is that the shift of the stripe is proportional to the difference of density. Hence, in two-dimensional flow, with appropriate parameters, the shift of the stripe becomes,

$$\Delta N = N_s(x, y) + F_i(\tilde{\rho} - 1) \tag{16}$$

where F_i is sensitivity of the interferogram system and shows how much difference of density corresponds to one stripe width. Density is normalized by freestream value for simplicity and denoted by $\tilde{\rho}$. One problem to generate interferogram

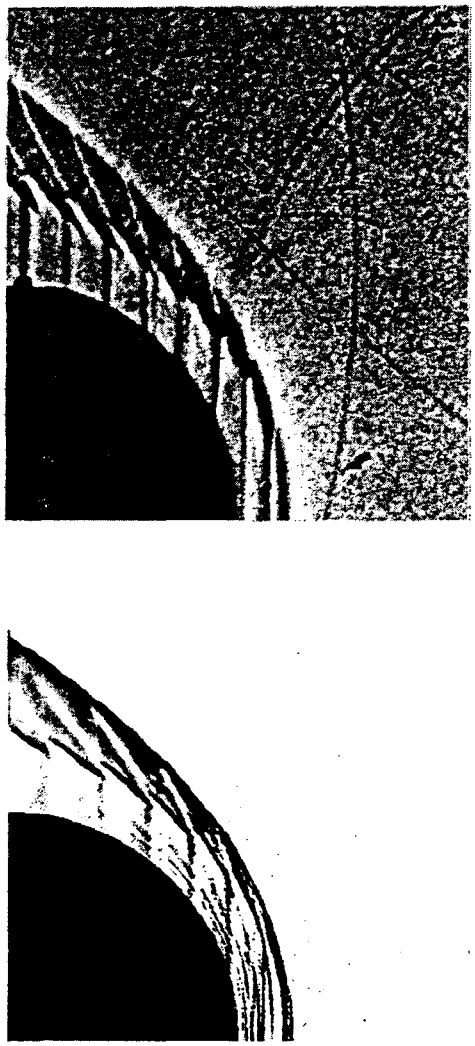

Figure 11 Shadowgraph of unsteady supersonic combustion around an axisymmetric blunt body (a) Experiment (Lehr (1972)). (b) Simulated result (Matsuo *et al.* (1991)).

image by a computer is that the obtained values are not colours nor lightness but the drifts of stripes. Since the fraction of ΔN corresponds to the dark and bright pattern, the lightness at the grid points can be calculated with the fraction of ΔN. However, the CG technique of a linear RGB interpolation within a grid, which is used for Schlieren photographs and shadowgraphs collapses when two or more stripes exist in one grid. For example, when $\Delta N_{j,k} = 0.0$ and $\Delta N_{j+1,k} = 2.0$, which means that there are two stripes between (j, k) and $(j+1, k)$, a linear RGB interpolation results in a flat colour paint inside the grid and does not paint two

(a)

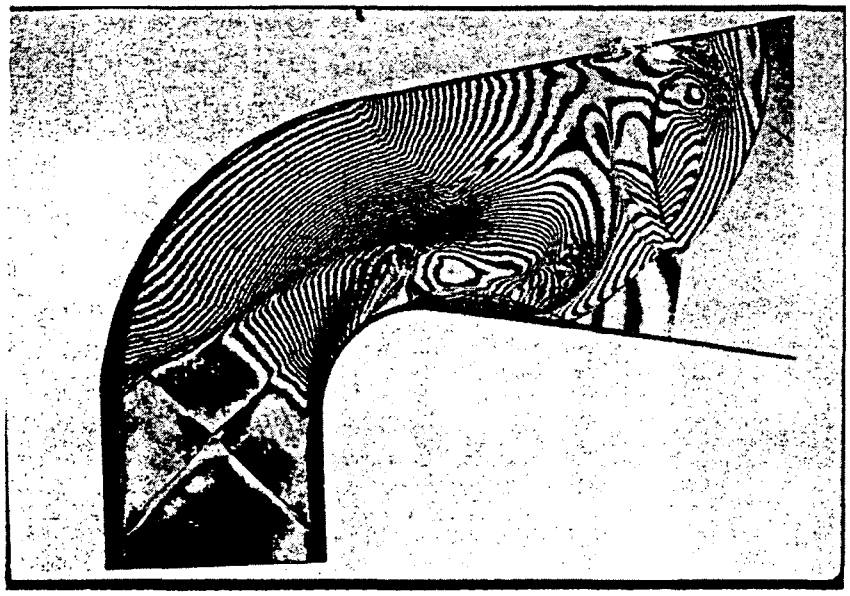

(b)

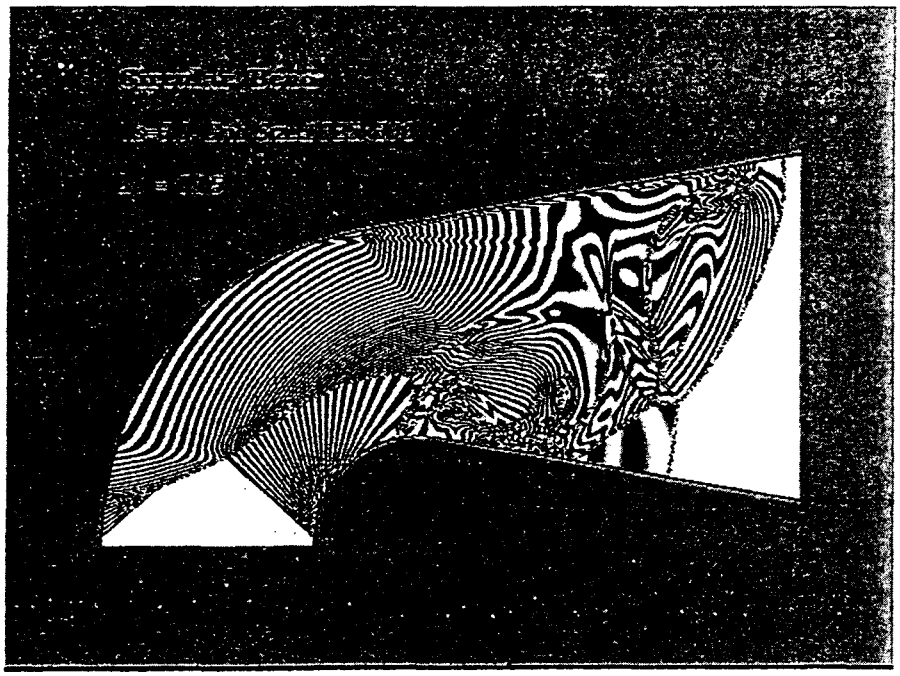

Figure 12 Unsteady shock wave in circular bend (Fursenko *et al.* (1991)) (a) Experimental interferogram pattern (b) Simulated interferogram pattern with computed result.

stripes. One can take more exact ways to paint it but it might take much longer CPU time. Simple interpolation may be sufficient when the grid spacing is fine enough or the interval of stripes is relatively large to the grid spacing, such that $|\Delta N_{j+1,k} - \Delta N_{j,k}| \ll 1.0$. Thus the simple interpolation is used here, although image at the region of strong density gradient, such as shock wave, cannot be exactly re-generated.

An unsteady flow field within a circular bend into which an incident shock wave passes through (Fursenko *et al.* (1991)) is taken as an example. Figure 12(a) shows interferogram pattern in the experiment and Figure 12(b) shows the simulated interferogram with the corresponding computed result. Since the number of grid points is large enough (1025×300), the obtained image is sufficiently resolved.

In three-dimensional flow, the differences of density are integrated along the ray as,

$$\Delta N = N_s(x, y) + F_i\left(\int_0^L \tilde{\rho}\, dz - 1\right) \tag{16)'}$$

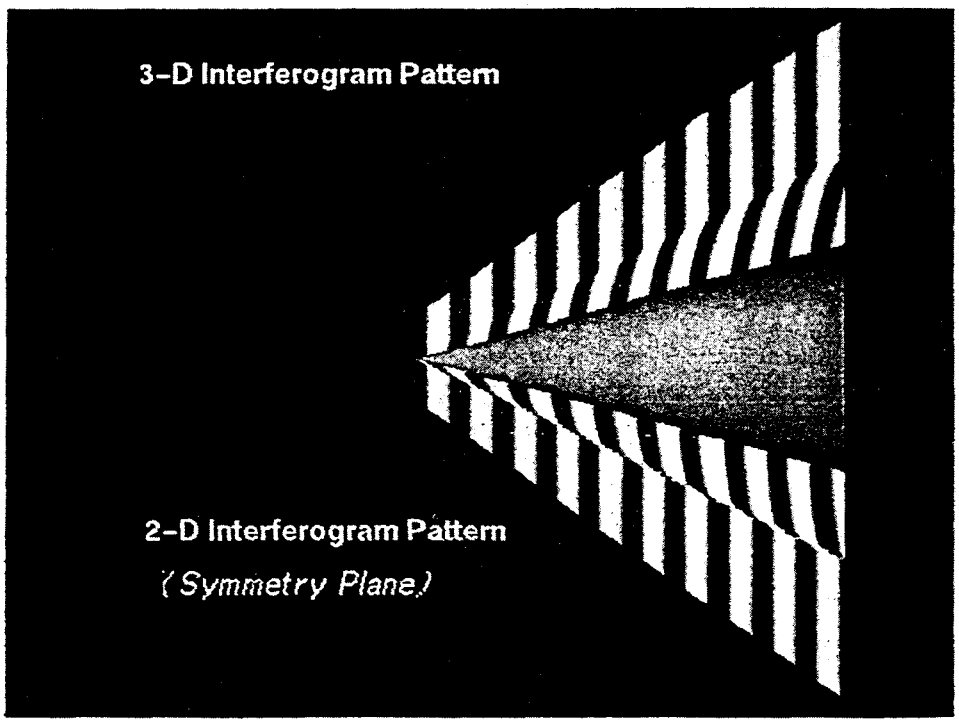

Figure 13 Simulated interferogram with computed result (Tamura *et al.* (1990a)) (a) Three-dimensional (b) Two-dimensional (symmetry plane).

The numerical integration is the same as Schlieren photograph and for one tetrahedron,

$$\rho_t = \tfrac{1}{2}\left[\tilde{\rho}_{\text{in}} + \tilde{\rho}_{\text{out}}\right] \times l_t \tag{17}$$

and as a result,

$$\int_0^L \tilde{\rho}\, \mathrm{d}z \approx \sum_t \rho_t$$

A three-dimensional example is a simulated interferogram pattern of a supersonic flow around a zero angle-of-attack cone and simulated two-dimensional interferogram pattern within symmetry plane is presented for comparison (Tamura *et al.* (1990a)), as shown in Figure 13.

3.4. Errors of Numerical Integration

In the case of three-dimensional simulations, errors tend to be accumulated because of the numerical interpolation and integration. Thus the accuracy of the numerical integration is evaluated in this section. Note that the error in this context is different from that of flow simulations. In the case of CFD, the values of computed results themselves are important, but in the case of visualization, what finally obtained are images. Thus the error to be discussed here is how different analyticaliy and numerically integrated images look and it is enough so far as these images look the same.

The images obtained by the analytical and numerical integration of a certain density distribution given by an analytical function are compared. The density distribution over the cone is given by an analytic (although not physical) function as,

$$\rho = \begin{cases} \rho_1 & : \quad 0 \leqslant r < x \tan\theta \\ \rho_2 + (\rho_1 - \rho_2)\dfrac{r - x\tan\theta}{\delta} & : \quad x\tan\theta \leqslant r < x\tan\theta + \delta \\ \rho_2 & : \quad x\tan\theta + \delta \leqslant r \end{cases} \tag{18-1}$$

$$\frac{\partial\rho}{\partial x} = \begin{cases} 0 & : \quad 0 \leqslant r < x\tan\theta \\ -(\rho_1 - \rho_2)\dfrac{\tan\theta}{\delta} = \text{const.} & : \quad x\tan\theta \leqslant r < x\tan\theta + \delta \\ 0 & : \quad x\tan\theta + \delta \leqslant r \end{cases} \tag{18-2}$$

where $r = \sqrt{y^2 + z^2}$, θ is shock angle, δ is width of shock wave. From Figure 14,

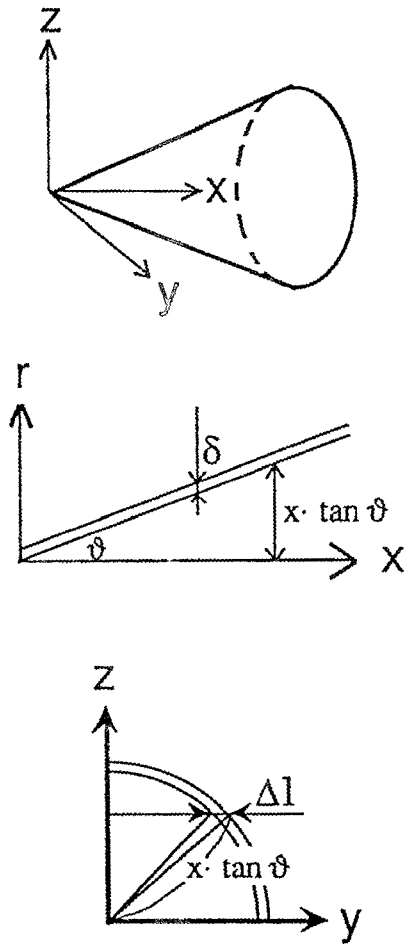

Figure 14 Density distribution testing numerical integration error.

density gradient in x direction by the analytical integration yields,

$$\int_0^\infty \frac{\partial \rho}{\partial x}\,dy = -(\rho_1 - \rho_2)\frac{\tan\theta}{\delta}\,\Delta l \tag{19}$$

$$\Delta l = \begin{cases} \sqrt{(x\tan\theta+\delta)^2 - z^2} - \sqrt{x^2\tan^2\theta - z^2} : & 0 \leqslant z < x\tan\theta \\ \sqrt{(x\tan\theta+\delta)^2 - x^2} : & x\tan\theta \leqslant x < x\tan\theta + \delta \\ 0 : & x\tan\theta + \delta \leqslant z \end{cases}$$

Figures 15 show the colour Schlieren pictures of density gradient obtained by the analytical and numerical integrations. The number of grid points is $51 \times 36 \times 51$.

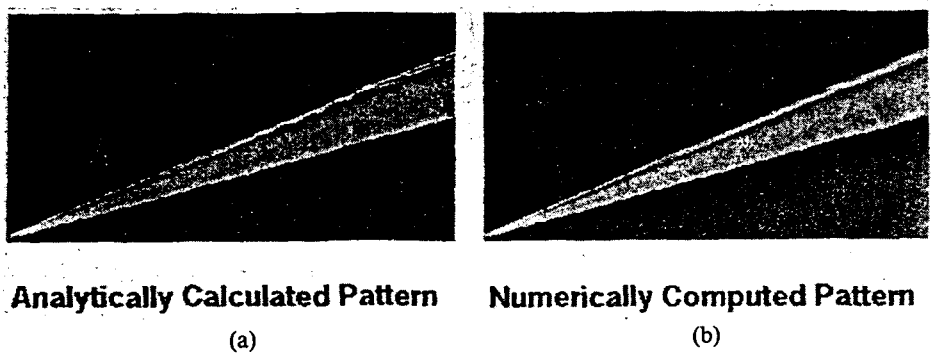

Figure 15 Error estimation of three-dimensional schlieren simulation (Tamura *et al.* (1990a)) (a) Obtained by analytic integration (b) Obtained by numerical integration. (See color plate III at the back of this issue.)

No difference can be recognized and the errors are negligible at least in this particular case.

4. NONLINEAR EFFECT OF DEFLECTION OF LIGHT

4.1. Estimation of Deflection of Light

In the second chapter, the light path is considered to be straight under the assumption that the deviation of density is small and thus the deflection angle is also small. When the deviation of density is relatively large and the light path is bent, the deflection of the light path Δy becomes (Figure 16),

$$\Delta y = \tan \phi \, \Delta z$$

Strictly speaking, $\partial\rho/\partial y$ in equation (3) is a function of y. However, $\partial\rho/\partial y$ is considered to be a sort of an averaged value here and thus constant for the order estimation. Then Δy can be integrated as,

$$y = \int \tan \phi \, dz = -\left(\frac{\beta}{n}\frac{\partial \rho}{\partial y}\right)^{-1} \log|\cos \phi| \tag{20}$$

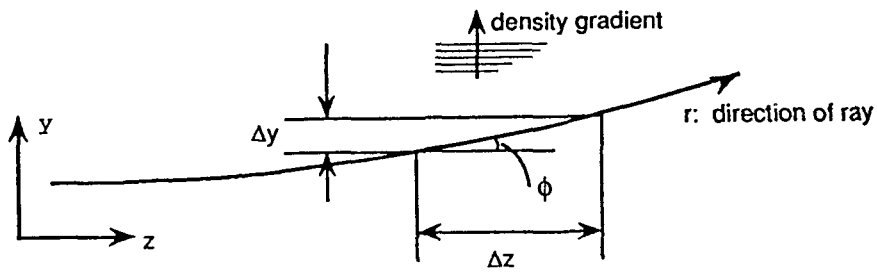

Figure 16 Non-linear distortion of ray.

When $\partial\rho/\partial y$ is taken to be order of 1, using $\beta \sim 0.0003$,

$$z \sim 1 \qquad y \sim 1.5 \times 10^{-4}$$

$$z \sim 10 \qquad y \sim 1.5 \times 10^{-2}$$

The length z can be considered as a distance of the test section in the lateral direction where density varies and $z \sim 1$ means that the object is three-dimensional and the scale of the region where density varies is about representative length at most. In this case, $y \sim 1.5 \times 10^{-4}$ and this non-linear effect is negligible. On the other hand, when flow is two-dimensional, the light possibly goes all the way through shock waves or boundary layers. In such a case, the deflection of light will be 1 percent or more.

4.2. Effect of Deflection of Light Path

In the case of Schlieren photographs, images are not distorted when the screen is exactly on the focal point. This is true when the light path is bent linearly. When the light is deflected non-linearly, not only the image shifts within a screen (the rate of shift is almost proportional to the deflection of light) but the focal point is drifted (Figure 17). When the focal point shifts, or the screen is not on the focal point from the beginning, the effect similar to shadowgraph is observed. In other words, higher- and lower-intensity region appears near regions of strong density gradients even without the knife edge. This effect is not obvious in a monochrome Schlieren picture using a knife edge because the lightness of the region is initially high or low enough to hide the effect. Even so, the brighter region just before the bow shock can be observed in Figure 18 (Van Dyke (1982)) and the cause might be this "shadowgraph" effect.

This is more obvious in the case of colour Schlierens. In these cases, the lightness

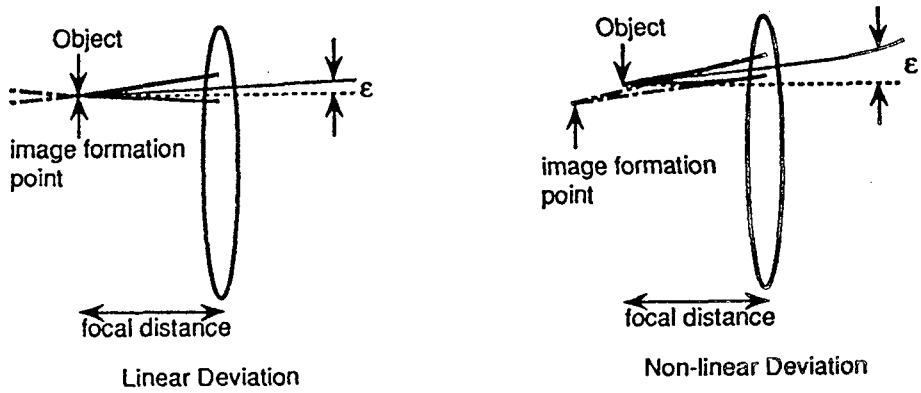

Figure 17 Drift of focal point by non-linear effects.

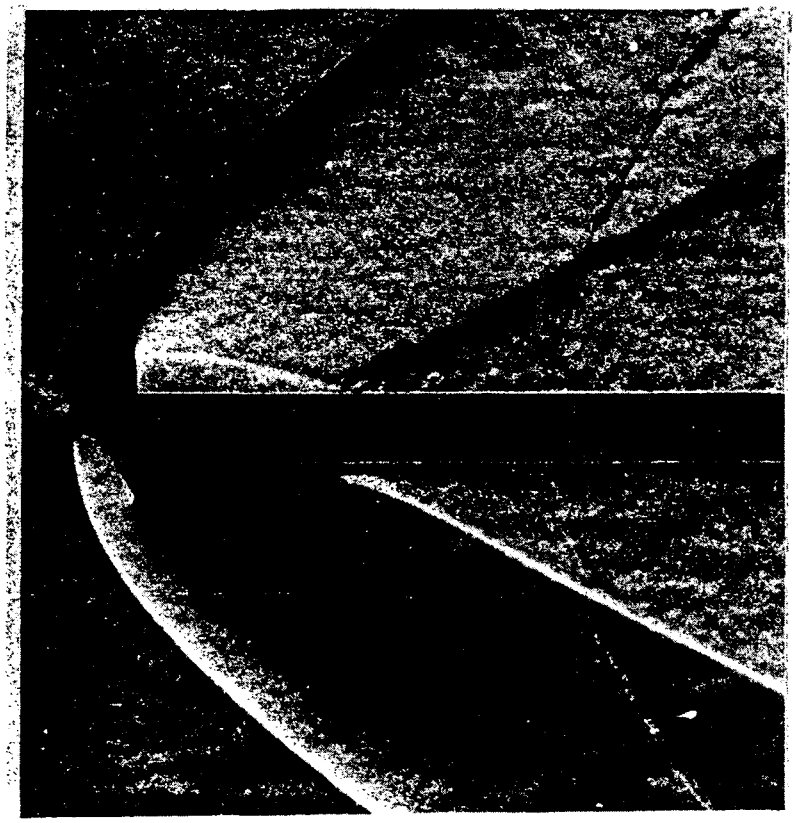

Figure 18 Example picture of Schlieren photograph which shows non-linear effects of deflection of light, Van Dyke (1982).

of the screen is ideally uniform since all of the light goes through the filter. When the light deflects too much, the light might illuminate the outside of the filter and the lightness on the screen might decrease. At least, no brighter regions must appear theoretically. However, Figure 9(a) shows a brighter region just after the shock wave, and dark-and-bright regions along the sting as if it indicates the density gradient which must not be captured with this filter alignment. In summary, one major non-linear effect of Schlieren photograph is the lightness deviation of "shadowgraph" effect.

Figure 19 shows the picture following the discussion above. The flow field is the two-dimensional supersonic intake (Kuroda *et al.* (1991)) presented in the previous section. Here hue H is followed by equation (11) and equation (15) gives the intensity which is constant in linear case.

Non-linearity of the deflection of light hardly affects the distortion of whole images since it is quite local and the rate of distortion is several percent at most. More than that, in colour Schlieren photograph, the deviation of lightness similar

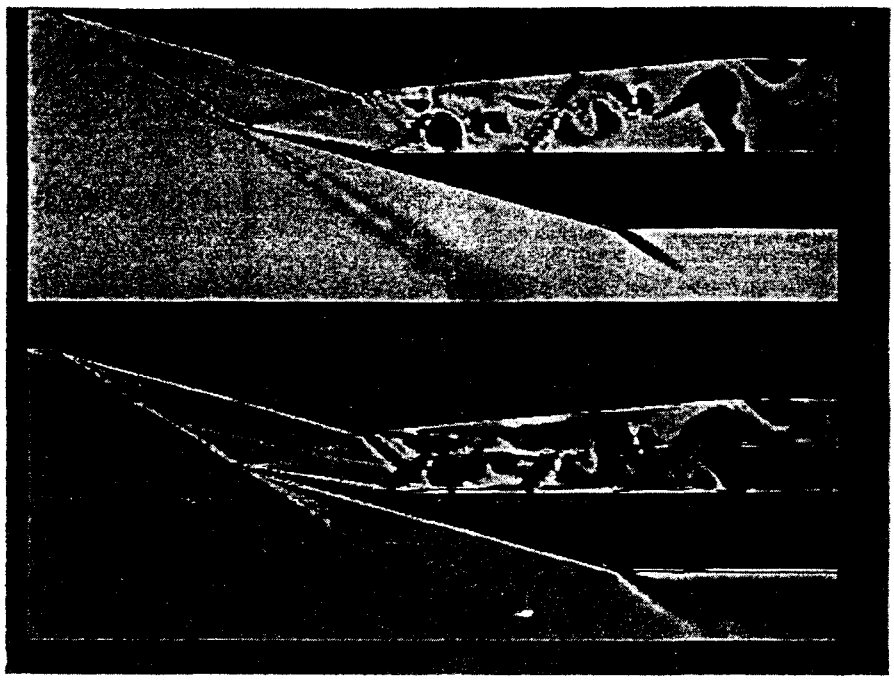

(a)

(b)

Figure 19 Effect of drift of focal point for simulated colour schlieren (a) Linear (b) Non-linear. (See color plate IV at the back of this issue.)

to shadowgraph caused by the drift of focal point changes the impression of the images. It might be important that the cause of the darkness near the shock wave could be "shadowgraph" effect and not be the out-of-range of the filter.

In the case of shadowgraphs, this non-linear effect, which shifts the practical focal point, is not so important as in the case of Schlieren photographs since the screen is located out of the focal point initially.

5. CONCLUDING REMARKS

From the viewpoint of comparisons with experiments, a method to simulate experimental visualization as postprocesses of computations is described. The present method enables more accurate comparisons between experiments and computations.

Postprocess has another purpose, that is to analyse computationally simulated flow fields. The method discussed here is useful for this purpose. Pictures in experiments such as Schlieren photograph is more familiar to us than the density contours and make us understand the flow fields more intuitively. For instance, flow features such as shock waves, expansion waves and shear layers are ambiguous in density contours (Figure 5(c)), but these features are highlighted in Schlieren photographs.

Considering non-linear effect of the deflection of light is important for the comparison with experiments. Although each experiment practically has its own error factors and it is difficult to reproduce them perfectly, the knowledge of non-linear effect is helpful to discuss the flow fields from the visualized images.

References

Furseno, A. A., Oshima, K., Sharov, D. M., Timofeev, E. V. and Voinovich, P. A. (1991) Numerical Simulation of Propagation of Shock Waves through Channel Bends Using TVD and ENO Scheme, A Collection of Technical Papers of the Fourth International Symposium on Computational Fluid Dynamics (4th ISCFD-Davis), 371–6.

Inatani, Y., Karashima, K., Fujii, K., Tanatsugu, N. and Abe, T. (1990) Newly Constructed High Speed Wind Tunnel at the Institute of Space and Astronautical Science (ISAS) and Related Activities, *AIAA Paper 90-5226, AIAA/NASP* 2nd International Aerospace Plane Conference.

Johanessen, N. H. (1952) *Philosophical Magazine*, **43**, 568–80.

Kuroda, S. and Fujii, K. (1991) Supersonic Inlet Flow Computations Using Fortified Navier-Stokes Approach, *AIAA Paper 91–1730, AIAA 22nd Fluid Dynamics, Plasma Physics and Laser Conference.*

Lear, H. F. (1972) Experiments on Shock-Induced Combustion, *Astronautica Acta*, **17**, 589–97.

Liepmann, H. W. and Roshko, A. (1956) *Element of Gas Dynamics*, John Wiley, New York, 153–79.

Matsuo, A. and Fujiwara, T. (1991) Numerical Simulation of Shock-Induced Combustion around an Axisymmetric Blunt Body, *AIAA Paper 91–1414, AIAA 22nd Fluid Dynamics*, Plasma Physics and Laser Conference.

Sakata, K., Yanagi, R., Shindo, S., Sakakibara, S., Hara, N., Honami, S., Shiraishi, K., Yasu, S. and Tanaka, A. (1989) Flow Visualization of Supersonic Air Intake, *Photographic Journal Album of Flow Visualization*, **6**, in Japanese.

Tamura, Y. and Fujii, K. (1990a) Visualization for Computational Fluid Dynamics and the Comparison with Experiments, *AIAA Paper 90–3031-CP*, AIAA 8th Applied Aerodynamics Conference.

Tamura, Y. and Fujii, K. (1990b) Visualization Method for Computational Fluid Dynamics with Emphasis on the Comparison with Experiments, *Proceedings of the 12th International Conference on Numerical Methods in Fluid Dynamics*, edited by K. W. Morton, Springer-Verlag, Berlin, Heidelberg, 406–10.

Tamura, Y. and Fujii, K. (1990c) Numerical Simulation of a Supersonic Experimental Model, *the 4th Symposium on Computational Fluid Dynamics*, 189–92, in Japanese.

Van Dyke, M. (1982) *An Album of Fluid Motion*, Parabolic Press, Stanford, California.